Influence of fluids on V_P/V_S ratio: increase or decrease?

Nicolas Brantut and Emmanuel C. David

Department of Earth Sciences, University College London, London WC1E 6BT, UK. E-mail: n.brantut@ucl.ac.uk

SUMMARY

The evolution of the ratio between *P*- and *S*-wave velocities (V_P/V_S) with increasing fluid-saturated porosity is computed for isotropic rocks containing spheroidal pores. The ratio V_P/V_S is shown to either decrease or increase with increasing porosity, depending on the aspect ratio α of the pores, fluid to solid bulk modulus ratio ζ and Poisson's ratio ν_0 of the solid constituents of the rock. A critical initial Poisson's ratio $\nu_{0,\,crit}$ is computed, separating cases where V_P/V_S increases (if $\nu_0 < \nu_{0,\,crit}$) or decreases (if $\nu_0 > \nu_{0,\,crit}$) with increasing porosity. For thin cracks and highly compressible fluids, $\nu_{0,\,crit}$ is approximated by $0.157\,\zeta/\alpha$, whereas for spherical pores $\nu_{0,\,crit}$ is given by $0.2 + 0.8\zeta$. When ν_0 is close to $\nu_{0,\,crit}$, the evolution of V_P/V_S with increasing fluid-saturated porosity is near neutral and depends on subtle changes in pore shape and fluid properties. This regime is found to be relevant to partially dehydrated serpentinites in subduction zones (porosity of aspect ratio near 0.1 and ζ in the range 0.01–0.1), and makes detection of these rocks and possibly elevated fluid pressures difficult from V_P/V_S only.

Key words: Wave propagation; Elasticity and anelasticity; Microstructure.

1 INTRODUCTION

The ratio of *P*- to *S*-wave velocities (V_P/V_S ratio) is commonly considered as a key constraint on the nature and composition of rocks when interpreting seismological data (e.g. Christensen 1996). It is also well established that the presence of fluid-filled porosity (cracks, pores or open grain junctions) strongly modifies the V_P/V_S ratio (e.g. Kuster & Toksöz 1974; O'Connell & Budiansky 1974; Watanabe 1993; Zimmerman 1994; Le Ravalec & Guéguen 1996; Berryman *et al.* 2002; Takei 2002; Fortin *et al.* 2007, among many others). Two systematic observations are that (1) full saturation leads to an increase in V_P/V_S compared to dry rocks (e.g. Nur & Simmons 1969), and (2) the opening of *liquid-saturated cracks* (e.g. when confining pressure is reduced) also causes an increase in V_P/V_S (see experimental data by Christensen 1984). Both observations are well supported by theoretical models based on effective medium schemes in cracked materials (e.g. O'Connell & Budiansky 1974; Berryman *et al.* 2002) and have been used to interpret results from seismic tomography (e.g. Peacock *et al.* 2011). However, when the fluid compressibility is very large compared to that of the rock, or when the fluid is present in pores shaped differently from thin cracks (e.g. tubes, spherical pores or polygonal grain-junctions), the change in V_P/V_S with increasing fluid-saturated porosity is not necessarily a monotonic increase. For instance, using an effective medium theory based on fluid inclusions in the shape of triangular tubes, Watanabe (1993) showed that, with increasing porosity, V_P/V_S initially decreases if the porosity is saturated with water, whereas it increases if the porosity is saturated with a much less compressible fluid such as melt. Similarly, the comprehensive review presented by

Takei (2002) shows that a regime exists where V_P/V_S decreases with increasing fluid content, notably for gas-saturated cracks (see also Dvorkin *et al.* 1999) and for texturally equilibrated water-saturated inclusions.

Overall, models based on effective medium approaches show that pore geometry and fluid compressibility have a strong influence on the variations in V_P/V_S (or, equivalently, Poisson's ratio) with increasing fluid content (e.g. O'Connell & Budiansky 1974; Zimmerman 1994; Berryman *et al.* 2002). However, an important control parameter that has been apparently overlooked is the Poisson's ratio of the host material. In most modelling studies, it is taken equal to 0.25 for simplicity, and a systematic exploration of this parameter has rarely been undertaken (a notable exception is Zimmerman 1991b, 1994, for the case of spherical inclusions). In addition, published models often require systematic computations of bulk and shear moduli as a function of fluid-saturated porosity to access the evolution in V_P/V_S, but it is desirable to achieve approximate predictions using simple formulae that exhibit clearly how the three key parameters (Poisson's ratio of solid constituents, pore shape and fluid compressibility) influence the results.

Here, we use the differential effective medium scheme to determine the variations of V_P/V_S in materials containing an isotropic distribution of fluid-filled spheroidal inclusions. We determine the critical parameter values separating cases when V_P/V_S increases or decreases with increasing porosity, and provide simple closed-form asymptotes for limiting pore shapes (cracks, spheres and needle-like cavities). Finally, we discuss a number of geophysically relevant cases where the presence of fluids may have a counterintuitive impact on V_P/V_S.

2 METHODOLOGY

We use (1) the differential effective medium (DEM) scheme to compute the effective elastic properties of solids containing voids (i.e. dry pores), and (2) the Gassmann relationship to compute the effect of a fluid filling the voids. Some of our analysis is given in the limit of small porosity (see Section 4.2) and is therefore general and does not rely specifically on the DEM approximation (Zimmerman 1991a).

The DEM approach consists in incrementally introducing inclusions (amounting to an increment of porosity), computing the corresponding incremental change in effective elastic moduli, and repeating the procedure until the target porosity is reached (e.g. Bruner 1976; McLaughlin 1977; Henyey & Pomphrey 1982; Zimmerman 1984; Norris 1985). For an isotropic solid containing randomly oriented, spheroidal voids of a given aspect ratio α, the effective bulk (K) and shear (G) moduli are given by the following set of coupled ordinary differential equations (e.g. David 2012)

$$\frac{1-\phi}{K}\frac{dK}{d\phi} = -P(\alpha, \nu), \tag{1}$$

$$\frac{1-\phi}{G}\frac{dG}{d\phi} = -Q(\alpha, \nu), \tag{2}$$

where ϕ is the porosity and ν is Poisson's ratio of the effective dry porous material. Poisson's ratio is related to the elastic moduli as

$$\nu = \frac{3K - 2G}{6K + 2G}. \tag{3}$$

The elastic constants of the intact material (at $\phi = 0$), that is, of the solid constituents of the rock matrix, are denoted K_0, G_0 and ν_0. The functions P and Q are the bulk and shear compliances of the spheroidal void, respectively, and depend on the Poisson's ratio ν of the dry porous solid, and the aspect ratio α of the spheroids. Full expressions for P and Q are given in David & Zimmerman (2011a). In using expressions (1) and (2), we assume the existence of a unique family of pores of the same representative aspect ratio α, and use the porosity ϕ as our control parameter. More complex microstructures could be represented by using a combination of pores of different aspect ratios, for instance mixtures of thin cracks and spherical pores, and using specific concentration parameters for each family (e.g. crack density and porosity, see Shafiro & Kachanov 1997). Here, we restrict our attention to a single aspect ratio in order to highlight the controlling role of this parameter and keep the analysis as simple as possible.

From the effective moduli of the dry porous material, the moduli of the fluid-saturated material are given by Gassmann's fluid-substitution relations in the undrained limit (Gassmann 1951):

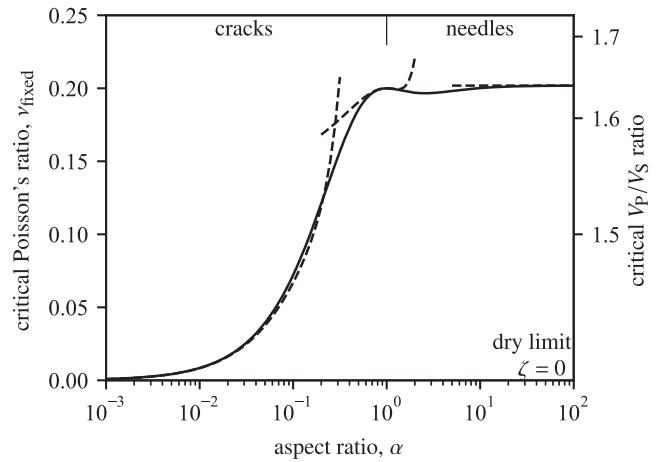$$K_u = K\frac{\phi(1 - \zeta^{-1}) + 1 - K_0/K}{\phi(1 - \zeta^{-1}) + K/K_0 - 1}, \tag{4}$$

$$G_u = G, \tag{5}$$

where subscripts u indicate saturated moduli, K is the dry effective bulk modulus and

$$\zeta = K_f/K_0 \tag{6}$$

is the ratio of the bulk moduli of the fluid and of the solid constituents of the material. From the elastic moduli, we compute Poisson's ratio using eq. (3) and the V_P/V_S ratio as

$$\frac{V_P}{V_S} = \sqrt{\frac{2(1 - \nu)}{1 - 2\nu}}. \tag{7}$$

Figure 1. Fixed point for Poisson's ratio and V_P/V_S as $\phi \to 1$ in the dry case. Low aspect ratios $\alpha < 1$ correspond to oblate spheroids (crack-like shapes), high aspect ratios $\alpha > 1$ correspond to prolate spheroids (needle-like shapes). Spheres correspond to $\alpha = 1$. The solid line is the numerical solution, and dashed lines are the closed-form asymptotes for thin cracks, spheres and needles.

3 DRY LIMIT

Before investigating the effect of fluids *per se*, it is instructive to examine first the evolution of V_P/V_S with increasing *dry* porosity. A full investigation was presented by David & Zimmerman (2011b), and only the key results are summarized here.

Combining eqs (3), (1) and (2), an ordinary differential equation for Poisson's ratio is obtained:

$$(1 - \phi)\frac{d\nu}{d\phi} = \frac{(1 + \nu)(1 - 2\nu)}{3}[Q(\alpha, \nu) - P(\alpha, \nu)]. \tag{8}$$

As shown in Berryman *et al.* (2002) and David & Zimmerman (2011b), Poisson's ratio evolves monotonically with increasing porosity towards a fixed point ν_{fixed} (where $d\nu/d\phi = 0$) that depends only on the aspect ratio of the pores, and is independent from the moduli of the solid constituents of the material. Qualitatively similar results hold for other effective medium schemes (e.g. Dunn & Ledbetter 1995). The fixed point ν_{fixed} can be computed by setting $Q(\alpha, \nu_{\text{fixed}}) = P(\alpha, \nu_{\text{fixed}})$, and is shown in Fig. 1 (solid line). Closed-form solutions in asymptotic cases (Appendix A) are obtained for

thin cracks ($\alpha \ll 1$):

$$\nu_{\text{fixed}} \simeq 0.861\alpha - 2.504\alpha^2 + 5.882\alpha^3, \tag{9}$$

nearly spherical pores ($\alpha \sim 1$):

$$\nu_{\text{fixed}} \simeq 0.200 - 0.018(1 - \alpha)^2 - 0.039(1 - \alpha)^3, \tag{10}$$

and needle-like pores ($\alpha \gg 1$):

$$\nu_{\text{fixed}} \simeq 0.202. \tag{11}$$

These asymptotic solutions (Fig. 1) show excellent agreement with the numerical solution over most of the aspect ratio range, except near the transition between thin cracks and spheres ($0.25 \lesssim \alpha \lesssim 0.6$) and between spheres and needles ($1.4 \lesssim \alpha \lesssim 11$). The asymptote for thin cracks (9) differs from that of Berryman *et al.* (2002) for penny-shaped cracks (their eq. B3) probably due to a typographical error [the asymptotic approximation given by Walsh (1969) for penny-shaped cracks—his eq. (1b)—does not match the one rederived in David & Zimmerman (2011a) in the dry case. Reconciling the two expressions requires removing the first unitary term

on the right-hand side of Walsh's eq. (1b)] propagated in the literature since Walsh (1969) (reproduced notably in Berryman 1980). The key result of the analysis, illustrated in Fig. 1, is that ν_{fixed} acts as a critical boundary separating materials (and pore shapes) for which increasing porosity produces a decrease or increase in ν (and V_P/V_S). When the Poisson's ratio of the intact material (i.e. that of the solid constituents of the rock) ν_0 is greater than $\nu_{\text{fixed}}(\alpha)$, then ν *decreases* with increasing porosity. In the example of thin cracks, $\nu_{\text{fixed}} \to 0$ as $\alpha \to 0$, so that Poisson's ratio is systematically decreasing with increasing crack porosity. Such a behaviour is confirmed by laboratory experiments on gas-saturated (or dry) cracked rocks (e.g. Dvorkin *et al.* 1999). Interestingly, *any* material for which $\nu_0 \gtrsim 0.2$ will see its Poisson's ratio decrease with increasing (dry) porosity, regardless of pore shape.

4 COMPRESSIBLE FLUIDS

4.1 General DEM results

At a given porosity, ν and V_P/V_S are always higher for the fluid-saturated porous solid than for its dry counterpart. This result is independent of the pore shape, and is a direct consequence of (1) the increase of K/G in the presence of fluids (Gassmann's eq. 4 and 5) and (2) ν being an increasing function of K/G.

When the porosity is saturated with a compressible fluid, the evolution in ν and V_P/V_S with increasing porosity differs significantly from the dry case. From a physical point of view, one expects that ν should tend to 0.5 ($V_P/V_S \to +\infty$) as $\phi \to 1$ (i.e. when the material is effectively just a fluid). For a saturating fluid of low compressibility, one also expects that ν should closely follow the evolution in the dry case at low porosity, before transitioning to an eventual increase towards 0.5 at high porosity. Such basic physical arguments indicate that the evolution of ν with porosity might be complex and non-monotonic.

Complete numerical solutions for the DEM combined with Gassmann's relationship are shown in Fig. 2. Each panel of Fig. 2 shows results for ν and V_P/V_S as function of porosity at fixed (α, ζ) and for $\nu_0 = 0.15$, 0.20, 0.25, 0.30 and 0.35. For thin cracks ($\alpha = 10^{-3}$, left panels), results are only shown for ϕ up to 1 per cent.

For thin cracks filled with a low compressibility fluid ($\alpha = 10^{-3}$, $\zeta = 10^{-2}$ and $\zeta = 10^{-1}$, Figs 2d and g), Poisson's ratio increases rapidly towards 0.5 as porosity increases to around 1 per cent, regardless of the solid's Poisson's ratio ν_0. For $\alpha = 10^{-3}$ and $\zeta = 10^{-3}$ (Fig. 2a), ν also rises rapidly to 0.5 at $\phi > 0.2$ per cent, but the initial evolution $\nu(\phi)$ depends on ν_0. For $\nu_0 = 0.15$, ν increases monotonically with increasing porosity. For $\nu_0 \geq 0.2$, the evolution at small porosity is a decrease in ν, followed by an increase at $\phi \geq 0.2$ per cent.

In the case of spherical pores ($\alpha = 1$, Figs 2c, f and i), the evolution of Poisson's ratio with increasing porosity depends on its initial value ν_0. For $\phi < 50$ per cent, ν increases if ν_0 is less than around 0.2, and decreases otherwise. At some large critical porosity (that depends on ζ), ν rapidly increases to 0.5. The strong variation of ν at ϕ near 100 per cent has been discussed in detail by Zimmerman (1994).

At intermediate aspect ratios ($\alpha = 0.1$, Figs 2b, e and h), ν typically evolves non-monotonically with increasing porosity. At low ζ ($\zeta \leq 10^{-2}$, highly compressible fluids), ν tends to decrease with increasing ϕ up to $\phi \approx 40$ per cent (at $\zeta = 10^{-3}$) and $\phi \approx 20$ per cent (at $\zeta = 10^{-2}$), before eventually increasing towards 0.5. For less compressible fluids ($\zeta = 10^{-1}$), the initial evolution of

ν strongly depends on ν_0: for $\nu_0 = 0.35$, $\nu(\phi)$ initially decreases, whereas it is either stable or increases at $\nu_0 \leq 0.3$.

4.2 Critical parameters separating increase from decrease in V_P/V_S

One way to understand the numerical results from the DEM approach is to determine the critical parameter values separating the cases where $d\nu/d\phi < 0$ and $d\nu/d\phi > 0$ at small ϕ, that is, at the introduction of fluid-saturated pores in the solid. We define a critical initial Poisson's ratio $\nu_{0,\,\text{crit}}(\alpha, \zeta)$ such that

$$\text{if} \quad \nu_0 > \nu_{0,\,\text{crit}} \quad \text{then} \quad \left.\frac{d\nu}{d\phi}\right|_{\phi=0} < 0. \tag{12}$$

Since $\nu_{0,\,\text{crit}}$ is defined in the limit $\phi \to 0$, the following analysis is not specific to the DEM approximation (when $\phi \to 0$, all effective medium schemes produce the same predictions).

The qualitative evolution of $\nu_{0,\,\text{crit}}$ with increasing aspect ratio is similar for all tested values of ζ (Fig. 3). At low α, $\nu_{0,\,\text{crit}}$ initially decreases with increasing aspect ratio, and then increases up to a plateau at $\alpha \geq 1$. The transition point where $\nu_{0,\,\text{crit}}$ is minimum scales with the ratio ζ/α. The value of $\nu_{0,\,\text{crit}}$ at aspect ratios above 1 depends on ζ but not significantly on α. For $\zeta \ll \alpha \ll 1$, the evolution of $\nu_{0,\,\text{crit}}$ closely follows that of ν_{fixed} in the dry case.

Asymptotic expressions for $\nu_{0,\,\text{crit}}$ can be determined in simple cases (see Appendix B):

thin cracks ($\alpha \ll \zeta \ll 1$):

$$\nu_{0,\text{crit}} \simeq 0.157 \frac{\zeta}{\alpha}, \tag{13}$$

spheres ($\alpha \sim 1$, $\zeta \ll 1$):

$$\nu_{0,\text{crit}} \simeq 0.2 + 0.8\zeta, \tag{14}$$

and needles ($\alpha \gg 1$, $\zeta \ll 1$):

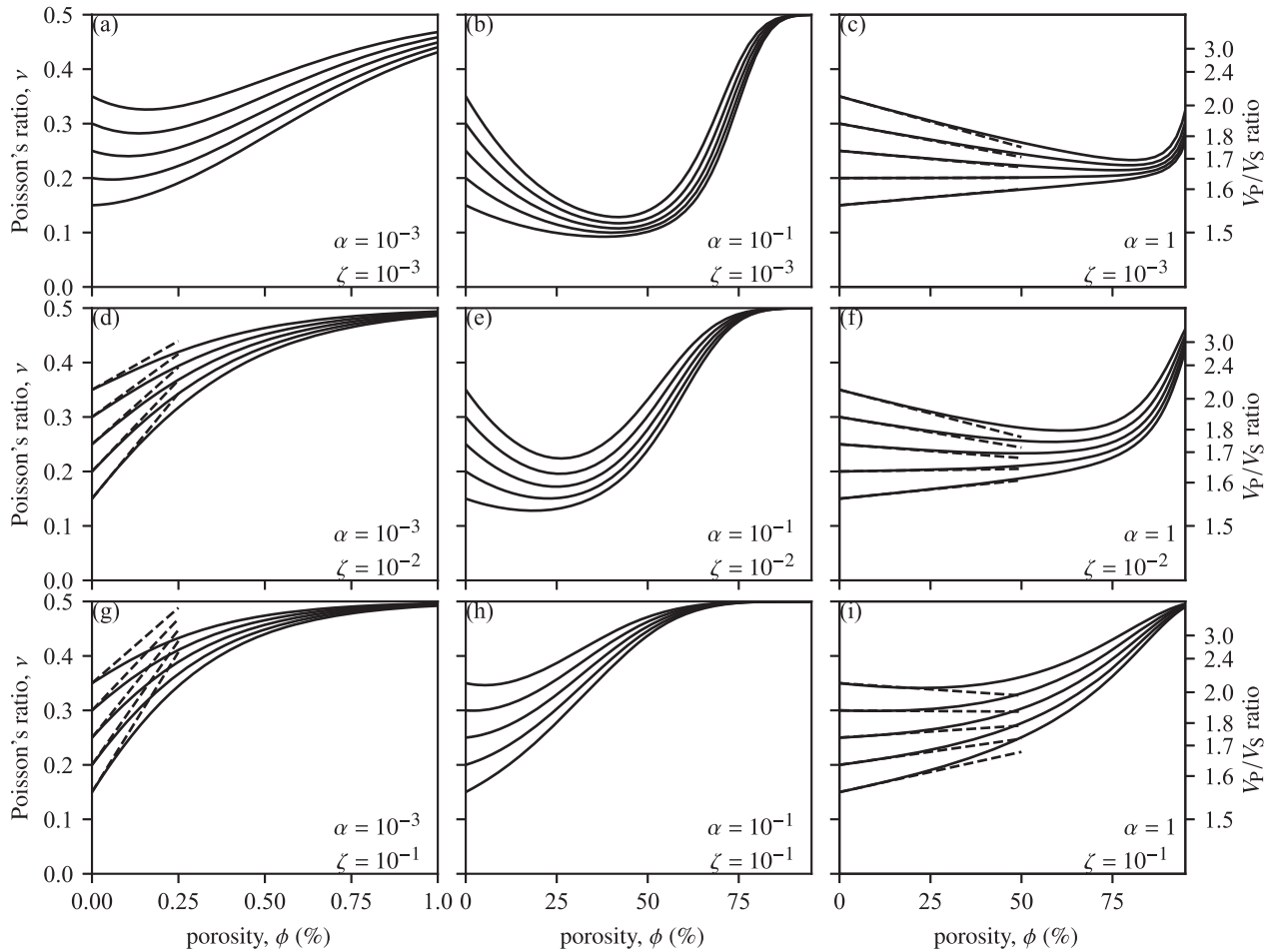$$\nu_{0,\text{crit}} \simeq 0.202 + 0.760\zeta. \tag{15}$$

The accuracy of these approximations is excellent at very low ζ, but deteriorates with increasing ζ, especially in the case of thin cracks (Fig. 3). More accurate asymptotes could probably be determined with higher order expansions in terms of α and ζ, but we retain formulae (13)–(15) because of their remarkable simplicity. For completeness, Appendix C presents analogue asymptotes for the case of fluid-saturated rocks in the high-frequency ('unrelaxed') limit and shows only small or no quantitative differences with eqs (13)–(15). The key result of our analysis, illustrated in Fig. 3, is the prediction and elementary estimate for the critical Poisson's ratio of solid constituents of a rock above which the introduction of fluid-saturated pores produces a *decrease* in the effective Poisson's ratio and V_P/V_S.

4.3 Estimates of V_P/V_S at low porosity

The comparison between Poisson's ratio of the solid constituents of the rock, ν_0, and $\nu_{0,\,\text{crit}}$, provides a simple rule to predict whether fluid-filled porosity induces an increase or a decrease in the effective ν of the saturated porous rock. The amplitude of the variation of ν with ϕ ($d\nu/d\phi$ at $\phi = 0$) is approximated by asymptotic expansions of the DEM and Gassmann's equations for

thin cracks ($\alpha \ll \zeta \ll 1$), $\nu_0 \lesssim 0.25$:

$$\left.\frac{d\nu}{d\phi}\right|_{\phi=0} \sim \frac{20 - 34\nu_0}{45\pi\alpha} + \frac{1 - \nu_0}{3}\left(1 - \frac{1}{\zeta}\right), \tag{16}$$

Figure 2. Evolution of Poisson's ratio and V_P/V_S with increasing fluid-saturated porosity for a range of pore aspect ratios ($\alpha = 10^{-3}$, 10^{-1} and 1) and fluid compressibility ratios ($\zeta = K_f/K_0 = 10^{-3}$, 10^{-2} and 10^{-1}). Solid lines are numerical solutions to the DEM and Gassmann's Equations (eqs 1, 2, 4 and 5) for initial Poisson's ratio ranging from $\nu_0 = 0.15$ to $\nu_0 = 0.35$. Dashed lines are asymptotic solutions obtained to first order in ϕ for thin cracks ($\alpha \ll \zeta \ll 1$) and spheres ($\alpha = 1$).

spheres ($\alpha = 1$, $\zeta \ll 1$):

$$\left.\frac{d\nu}{d\phi}\right|_{\phi=0} \sim \frac{3}{2}\frac{(1-5\nu_0)(1-\nu_0^2)}{7-5\nu_0} + \frac{3}{4}\frac{(1-\nu_0)^2(1+\nu_0)}{1-2\nu_0}\zeta, \qquad (17)$$

and needles ($\alpha \gg 1$, $\zeta \ll 1$):

$$\left.\frac{d\nu}{d\phi}\right|_{\phi=0} \sim \frac{(1+\nu_0)(5-28\nu_0+16\nu_0^2)}{15} + \frac{(1+\nu_0)(5-4\nu_0)^2}{27(1-2\nu_0)}\zeta. \quad (18)$$

Linear approximation for $\nu(\phi)$ at small porosities using the above asymptotes are shown as dashed lines in Fig. 2. The approximation for spheres is remarkably accurate up to very large porosity (ϕ up to 25 per cent), while the approximation for thin cracks becomes poor at porosity larger than 0.1 per cent. More accurate, higher order asymptotes for the case of thin cracks could be obtained, but we only retain here the very approximate formula (16) for its simplicity, keeping in mind that full numerical solutions should be used at high crack porosity, large ζ and $\nu_0 \gtrsim 0.25$.

5 DISCUSSION

Our modelling results demonstrate that the evolution in ν (or, equivalently, V_P/V_S) with increasing fluid-saturated porosity is potentially non-monotonic. The critical initial Poisson's ratio $\nu_{0, \text{crit}}$ separating cases when V_P/V_S decreases or increases shows a complex evolution

at pore aspect ratios near $\alpha = 0.1$ and fluid compressibility ratios near $\zeta = 0.1$. This range of parameters is typical of two key scenarios of geological relevance: metamorphic dehydration reactions and partial melting.

The laboratory experiments of Popp & Kern (1993) and Brantut *et al.* (2012) showed that both serpentinite and gypsum undergoing thermal dehydration reactions see their Poisson's ratio *decrease* with increasing reaction progress (i.e. with increasing fluid-saturated porosity). More specifically, Brantut *et al.* (2012) used the DEM approach to show that the pores generated by the transformation of gypsum to bassanite have an aspect ratio of the order of 0.05. This relatively large value is required due to the large porosity generated by dehydration reactions (typically of the order of 10 per cent or more), which cannot be accommodated by thin cracks only (Brantut *et al.* 2012). Takei (2002) showed that equilibrated textures for partially molten and fluid-saturated rocks, where porosity is located at grain boundaries and triple junctions and is in equilibrium with surface tension forces, correspond to an effective material containing spheroidal pores of aspect ratio $\alpha = 0.1$–0.5.

Using intact Poisson's ratio of $\nu_0 = 0.33$–0.35 for gypsum (Brantut *et al.* 2012), $\nu_0 = 0.31$–0.33 for lizardite (Popp & Kern 1993; Christensen 1996) and $\nu_0 = 0.26$–0.28 for antigorite (Reynard 2013), the evolution of ν and V_P/V_S of these rocks at the onset of dehydration is in a regime where it is strongly controlled by the
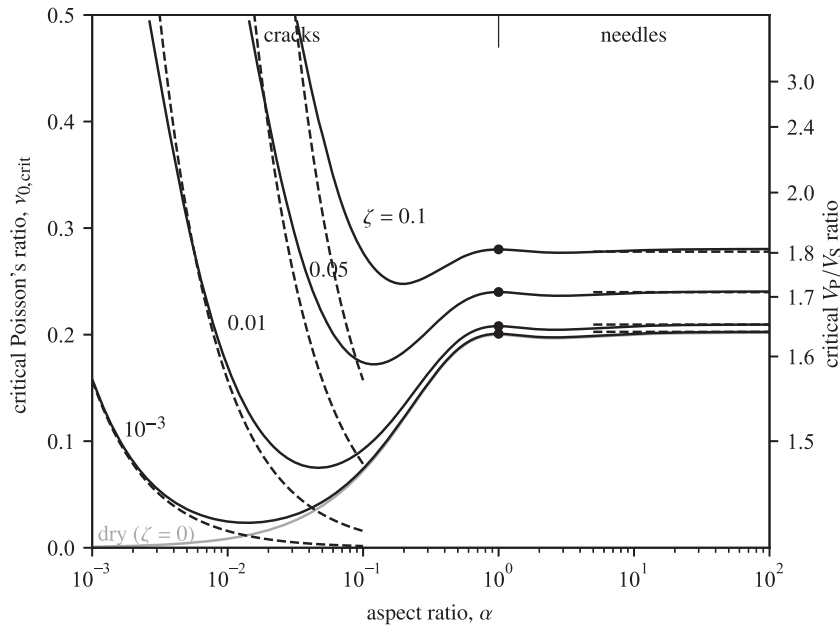
Figure 3. Critical initial Poisson's ratio and V_P/V_S separating increasing or decreasing $\nu(\phi)$ at $\phi = 0$. For $\nu_0 > \nu_{0,\,\text{crit}}$, ν (and V_P/V_S) initially decreases with increasing fluid-saturated porosity. Solid lines are numerical solutions. Dashed lines and black circles are asymptotic closed-form expressions for thin cracks, needle-like pores and spherical pores, respectively. The solid grey curve corresponds to the dry case (same as in Fig. 1).
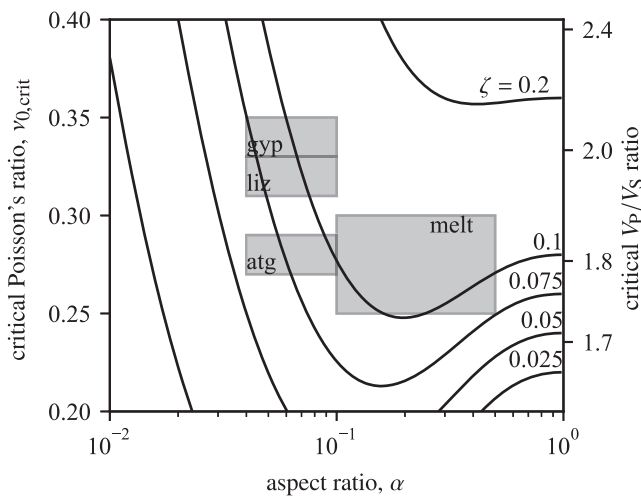
Figure 4. Critical Poisson's ratio and V_P/V_S as a function of aspect ratio and for indicated compressibility ratios $\zeta = 0.02$–0.2. Grey boxes correspond to (α, ν_0) ranges at the onset of gypsum dehydration (gyp), lizardite dehydration (liz), antigorite dehydration (atg) and silicate melting (melt).

compressibility ratio ζ (Fig. 4). Gypsum dehydration occurs at low pressure and temperature, so that $K_f \approx 2$ GPa and $K_0 \approx 41$ GPa, yielding $\zeta \approx 0.05$. This set of parameters is clearly in the regime where $\nu_0 > \nu_{0,\,\text{crit}}$, and Poisson's ratio is expected to decrease with increasing porosity, a prediction confirmed by experiments (Brantut *et al.* 2012). For the case of lizardite dehydration at around 400 °C, the evolution of ν depends on the fluid pressure. Under the experimental conditions of the study by Popp & Kern (1993), the fluid pressure is expected to be commensurate to the confining pressure of 200 MPa, so that the bulk modulus of water is of the order of 1 GPa (at 400 °C). Using $K_0 \approx 57$ GPa (derived from Christensen 1996), it is found that $\zeta \approx 0.02$, well within the regime where $\nu_0 > \nu_{0,\,\text{crit}}$, so that ν decreases with increasing porosity, as confirmed by the experimental results. By contrast, if lizardite dehydration occurs

at higher pressure, say 1 GPa, the fluid bulk modulus is around $K_f \approx 5.5$ GPa, so that $\zeta \approx 0.1$, and the resulting evolution of ν and V_P/V_S is neutral (at α near 0.1) or increasing (at $\alpha \lesssim 0.07$). Similarly, the case of antigorite dehydration is also complex. At 1 GPa pressure and 550 °C, the bulk modulus of water is $K_f \approx 4.5$ GPa. Using a bulk modulus of $K_0 \approx 75$ GPa for pure antigorite (Bezacier *et al.* 2013) results in $\zeta \approx 0.06$, which places ν_0 only slightly above $\nu_{0,\,\text{crit}}$. Therefore, antigorite dehydration is expected to produce *constant* or slightly *decreasing* ν and V_P/V_S.

By contrast, the case of partial melting of silicates is unambiguous. Using a lower crustal silicate melt compressibility in the range 18–27 GPa (Stolper *et al.* 1981) and silicate bulk modulus in the range 80–110 GPa yields $\zeta \approx 0.16$–0.34. For most silicate rocks, ν_0 is in the range 0.2–0.3, which is below the predicted $\nu_{0,\,\text{crit}}$ for melt-saturated pores (Fig. 4), so that partial melting is expected to produce an increase in ν and V_P/V_S, in accordance with previous predictions by Takei (2002).

6 CONCLUSIONS

The results from the DEM approach demonstrate that the Poisson's ratio ν_0 of the solid constituents of a rock exerts a key control on the evolution of ν and V_P/V_S with increasing fluid-saturated porosity. This control has often been overlooked and most modelling studies have instead focused on the effect of pore shape and fluid compressibility, assuming $\nu_0 = 0.25$. Here, we computed a critical Poisson's ratio $\nu_{0,\,\text{crit}}(\alpha, \zeta)$ separating the cases when ν (and V_P/V_S) *decreases* (if $\nu_0 > \nu_{0,\,\text{crit}}$) or increases (if $\nu_0 < \nu_{0,\,\text{crit}}$) with increasing porosity. Our analysis of $\nu_{0,\,\text{crit}}$ is given in the limit of small porosity, and is therefore independent from the choice of a specific effective medium scheme. Simple asymptotic formulae were derived in the case of thin cracks, spherical pores and needle-like pores (eqs (13), (14) and (15)). When ν_0 is very close to $\nu_{0,\,\text{crit}}$, the evolution of V_P/V_S with porosity is near neutral, but becomes sensitive to subtle changes in pore shape and fluid compressibility. This case is likely

encountered during dehydration reactions of serpentinites, where the details of the pore shape (driven by textural equilibration of the microstructure) and fluid properties (which depend on the local pressure, temperature and chemical composition) are expected to drive V_P/V_S towards either a slight increase or a decrease. A significant decrease in V_P/V_S was observed during lizardite dehydration (Popp & Kern 1993) in accordance to our model's prediction. More experimental work is needed to further test the model predictions over a wider range of conditions and materials.

We only treated the case of isotropic solids containing isotropic distributions of pore orientations. Anisotropic matrix or anisotropic pore orientation distributions are expected to change the expected V_P/V_S ratio which then depends on the polarization of the seismic waves propagating through the material (Reynard *et al.* 2010; Wang *et al.* 2012). In natural scenarios, such as partially dehydrated rocks in subduction zones, the combined effects of initial rock properties, fluid properties, pore shape and anisotropy make structural interpretations difficult from the measurement of V_P/V_S only. Unambiguous identification of specific rock types (such as serpentinites) and locally elevated fluid pressures is therefore likely to require a combination of data sets, including wave speed anisotropy and attenuation.

ACKNOWLEDGEMENTS

REFERENCES

Berryman, J., Pride, S. & Wang, H., 2002. A differential scheme for elastic properties of rocks with dry or saturated cracks, *Geophys. J. Int.,* **151,** 597–611.

Berryman, J.G., 1980. Long-wavelength propagation in composite elastic media II. Ellipsoidal inclusions, *J. acoust. Soc. Am.,* **68**(6), 1820–1831.

Bezacier, L., Reynard, B., Cardon, H., Montagnac, G. & Bass, J.D., 2013. High-pressure elasticity of serpentine and seismic properties of the hydrated mantle wedge, *J. geophys. Res.,* **118,** 527–535.

Brantut, N., David, E.C., Schubnel, A., Héripré, E., Guéguen, Y. & Dimanov, A., 2012. Dehydration-induced damage and deformation in gypsum and implications for subduction zone processes, *J. geophys. Res.,* **117,** B03205, doi:10.1029/2011JB008730.

Bruner, W., 1976. Comment on 'Seismic velocities in dry and saturated cracked solids' by Richard J. O'Connell and Bernard Budiansky, *J. geophys. Res.,* **81,** 2573–2576.

Christensen, N.I., 1984. Pore pressure and oceanic crustal seismic structure, *Geophys. J. R. astr. Soc.,* **79,** 411–423.

Christensen, N.I., 1996. Poisson's ratio and crustal seismology, *J. geophys. Res.,* **101**(B2), 3139–3156.

David, E.C., 2012. The effect of stress, pore fluid and pore structure on elastic wave velocities in sandstones, *PhD thesis,* Imperial College London, London.

David, E.C. & Zimmerman, R.W., 2011a. Compressibility and shear compliance of spheroidal pores: exact derivation via the Eshelby tensor, and asymptotic expressions in limiting cases, *Int. J. Solids Struct.,* **48,** 680–686.

David, E.C. & Zimmerman, R.W., 2011b. Elastic moduli of solids containing spheroidal pores, *Int. J. Eng. Sci.,* **49**(7), 544–560.

Dunn, M. & Ledbetter, H., 1995. Poisson's ratio of porous and microcracked solids: theory and application to oxide superconductors, *J. Mater. Res.,* **10,** 2715–2722.

Dvorkin, J., Mavko, G. & Nur, A., 1999. Overpressure detection from compressional- and shear-wave data, *Geophys. Res. Lett.,* **26**(22), 3417–3420.

Fortin, J., Guéguen, Y. & Schubnel, A., 2007. Effects of pore collapse and grain crushing on ultrasonic velocities and V_p/V_s, *J. geophys. Res.,* **112,** B08207, doi:10.1029/2005JB004005.

Gassmann, F., 1951. Über die Elastizität poröser Medien, *Vierteljahrsschrift der Naturforschenden Gesellschaft in Zürich,* **96,** 1–23.

Henyey, F.S. & Pomphrey, N., 1982. Self-consistent elastic moduli of a cracked solid, *Geophys. Res. Lett.,* **9**(8), 903–906.

Kuster, G.T. & Toksöz, M.N., 1974. Velocity and attenuation of seismic waves in two-phase media: Part I. Theoretical formulations, *Geophysics,* **39,** 587–606.

Le Ravalec, M. & Guéguen, Y., 1996. High- and low-frequency elastic moduli for a saturated porous/cracked rock–Differential self-consistent and poroelastic theories, *Geophysics,* **61,** 1080–1094.

Li, Y., David, E.C., Nakagawa, S., Kneafsey, T.J., Schmitt, D.R. & Jackson, I., 2018. A broadband laboratory study of the seismic properties of cracked and fluid-saturated synthetic glass media, *J. geophys. Res.,* **123,** 3501–3538.

McLaughlin, R., 1977. A study of the differential scheme for composite materials, *Int. J. Eng. Sci.,* **15,** 237–244.

Norris, A.N., 1985. A differential scheme for the effective moduli of composites, *Mech. Mater.,* **4,** 1–16.

Nur, A. & Simmons, G., 1969. The effect of saturation on velocity in low porosity rocks, *Earth planet. Sci. Lett.,* **7,** 183–193.

O'Connell, R.J. & Budiansky, B., 1974. Seismic velocities in dry and saturated cracked solids, *J. geophys. Res.,* **79**(35), 5412–5426.

Peacock, S.M., Christensen, N.I., Bostock, M.G. & Audet, P., 2011. High pore pressures and porosity at 35 km depth in the Cascadia subduction zone, *Geology,* **39**(5), 471–474.

Popp, T. & Kern, H., 1993. Thermal dehydration reactions characterised by combined measurements of electrical conductivity and elastic wave velocities, *Earth planet. Sci. Lett.,* **120,** 43–47.

Reynard, B., 2013. Serpentine in active subduction zones, *Lithos,* **178,** 171–185.

Reynard, B., Nakajima, J. & Kawakatsu, H., 2010. Earthquakes and plastic deformation of anhydrous slab mantle in double Wadati-Benioff zones, *Geophys. Res. Lett.,* **37,** L24309, doi:10.1029/2010GL045494.

Shafiro, B. & Kachanov, M., 1997. Materials with fluid-filled pores of various shapes: effective elastic properties and fluid pressure polarization, *Int. J. Solids Struct.,* **34**(27), 3517–3540.

Stolper, E., Walker, D., Hager, B.H. & Hays, J.F., 1981. Melt segregation from partially molten source regions: the importance of melt density and source region size, *J. geophys. Res.,* **86**(B7), 6261–6271.

Takei, Y., 2002. Effect of pore geometry on V_P/VS: from equilibrium geometry to crack, *J. geophys. Res.,* **107**(B2), 2043, doi:10.1029/2001JB000522.

Walsh, J.B., 1969. New analysis of attenuation in partially melted rock, *J. geophys. Res.,* **74**(17), 4333–4337.

Wang, X.-Q., Schubnel, A., Fortin, J., David, E.C., Guéguen, Y. & Ge, H.-K., 2012. High *V*p/*V*s ratio: saturated cracks of anistropy effects?, *Geophys. Res. Lett.,* **39,** L11307, doi:10.1029/2012GL051742.

Watanabe, T., 1993. Effects of water and melt on seismic velocities and their application to characterization of seismic reflectors, *Geophys. Res. Lett.,* **20**(24), 2933–2936.

Zimmerman, R., 1984. Elastic moduli of a solid with spherical pores: new self-consistent method, *Int. J. Rock Mech. Min. Sci. Geomech. Abstr.,* **21,** 339–343.

Zimmerman, R.W., 1991a. *Compressibility of Sandstones,* Elsevier.

Zimmerman, R.W., 1991b. Elastic moduli of a solid containing spherical inclusions, *Mech. Mat.,* **12,** 17–24.

Zimmerman, R.W., 1994. Behavior of the Poisson ratio of a two-phase composite material in the high-concentration limit, *Appl. Mech. Rev.,* **47**(1), S38–S44.

APPENDIX A: ASYMPTOTIC FORMS IN THE DRY CASE

The fixed point ν_{fixed} is given by solving for ν in

$$Q(\alpha, \nu) - P(\alpha, \nu) = 0. \tag{A1}$$

Thin cracks ($\alpha \ll 1$). The term $Q(\alpha, \nu) - P(\alpha, \nu)$ is a rational function of the variable ν. Removing the unphysical root $\nu = 1$, retaining the two dominant terms of order zero and one in ν, and performing a Taylor expansion to third order in α yield the approximation

$$\nu_{\text{fixed}} \sim \left(\frac{4}{3\pi} + \frac{5\pi}{36}\right)\alpha + \left(-\frac{254}{81} + \frac{80}{27\pi^2} + \frac{29\pi^2}{864}\right)\alpha^2$$
$$+ \frac{(1228800 + 1660160\pi^2 + 165504\pi^4 + 315\pi^6)}{186624\pi^3}\alpha^3. \tag{A2}$$

Nearly spherical pores ($\alpha \sim 1$). Taylor expansion of $P(\alpha, \nu)$ and $Q(\alpha, \nu)$ for $\epsilon = (1 - \alpha) \sim 0$ is used, and eq. (A1) is then solved to yield a third-order approximation in ϵ as

$$\nu_{\text{fixed}} \sim \frac{1}{5} - \frac{16}{875}\epsilon^2 + \frac{3017088\left(5751377 + 23283\sqrt{59385}\right)}{42875\left(135 + \sqrt{59385}\right)^4}\epsilon^3. \tag{A3}$$

Needles ($\alpha \gg 1$). The limits of P and Q for needles (see David & Zimmerman 2011a) are used, and the solution of eq. (A1) gives

$$\nu_{\text{fixed}} \sim \frac{1}{8}\left(7 - \sqrt{29}\right), \tag{A4}$$

recovering the solution previously derived by Berryman *et al.* (2002).

APPENDIX B: ASYMPTOTIC FORMS IN THE SATURATED, UNDRAINED CASE

Here we only study the behaviour at small porosity, near $\phi = 0$. The set of eqs (1) and (2) for the DEM scheme then reduces to the dilute approximation:

$$K_0/K = 1 + \phi P(\alpha, \nu), \tag{B1}$$

$$G_0/G = 1 + \phi Q(\alpha, \nu). \tag{B2}$$

The first (and most obvious) method for evaluating $\nu_{0, \text{crit}}$ in the fluid-saturated case would be to (1) insert the asymptotic expressions of David & Zimmerman (2011a) for P and Q in limiting cases of thin cracks, nearly spherical pores and needles in eqs (B1) and (B2) to compute the dry moduli in the limit of small porosity, (2) use Gassmann's equation to compute the saturated moduli and (3) solve for $\nu_{0, \text{crit}}$ for each pore geometry. However, we found this approach rather cumbersome. Alternatively, the fluid-saturated Poisson ratio is readily evaluated by solving a modified DEM scheme in the limit of small porosity, using the shear compliance of dry pores Q (unaffected by fluid saturation in the low frequency limit) and an effective pore bulk compliance equal to $(1 - \zeta)P_u(\alpha, \nu, \zeta)$, where P_u is the bulk compliance of fluid-saturated inclusions (David 2012). This approach has been shown to be rigorously equivalent to the first method described above in the limit of small porosity (David

2012). The critical Poisson's ratio is given by setting

$$Q(\alpha, \nu) - (1 - \zeta)P_u(\alpha, \nu, \zeta) = 0. \tag{B3}$$

Thin cracks ($\alpha \ll 1$). Series expansions of P_u and Q for small α and small ζ (in that order) are used, and yield the following approximation:

$$\nu_{0,\text{crit}} \sim \frac{40\zeta}{81\pi\alpha}. \tag{B4}$$

Because of the order in which the series expansions are performed, this approximation is valid for $\alpha \ll \zeta$. We did not find any useful approximation for the case $\zeta \leq \alpha \ll 1$.

Spheres ($\alpha \sim 1$). Series expansions near $\alpha = 1$ and small ζ result in an approximation that is independent from α (at least to first order):

$$\nu_{0,\text{crit}} \sim \frac{1}{5}\left(1 + 4\zeta\right). \tag{B5}$$

Needles ($\alpha \gg 1$). Series expansions for large α and small ζ yield

$$\nu_{0,\text{crit}} \sim \frac{1}{8}\left(7 - \sqrt{29}\right) + \frac{203 + 36\sqrt{29}}{522}\zeta. \tag{B6}$$

APPENDIX C: ASYMPTOTIC FORMS IN THE SATURATED, UNRELAXED CASE

In the previous Section we derived asymptotes for the undrained saturated case, which is given by inserting the dry moduli from the DEM scheme into Gassmann's equations. The undrained case corresponds to the low-frequency limit (Le Ravalec & Guéguen 1996), where the fluid pressure is the same in all pores within a representative elementary volume over which the averaging procedure is performed. In the high-frequency limit, also called 'unrelaxed' or 'saturated-isolated' limit, the fluid pressure is not equilibrated between each pore. This results in saturated effective moduli that are equal or higher than those predicted in the undrained, low-frequency regime (Le Ravalec & Guéguen 1996). Although this case is commonly not directly relevant to the low frequencies used in conventional seismology (Li *et al.* 2018), for completeness we include here the key asymptotes for $\nu_{0, \text{crit}}$ for each aspect ratio limit. Although the evolution of ν with increasing ϕ is quantitatively different compared to the undrained, low-frequency case, only minor differences are found for the critical Poisson ratio $\nu_{0, \text{crit}}$.

The high frequency, unrelaxed critical Poisson's ratio $\nu_{0,\text{crit}}^{\text{HF}}$ is given by setting

$$Q_u(\alpha, \nu, \zeta) - (1 - \zeta)P_u(\alpha, \nu, \zeta) = 0, \tag{C1}$$

where Q_u is the shear compliance of a fluid-saturated spheroidal inclusion (see David 2012, for complete expression).

Thin cracks ($\alpha \ll 1$). Series expansions of P_u and Q_u for small α and small ζ (in that order) are used, and yield the following approximation:

$$\nu_{0,\text{crit}}^{\text{HF}} \sim \frac{8\zeta}{27\pi\alpha} \simeq 0.094\,\zeta/\alpha. \tag{C2}$$

Spheres ($\alpha \sim 1$). This case is rigorously equivalent to the undrained case:

$$\nu_{0,\text{crit}}^{\text{HF}} \sim \frac{1}{5}\left(1 + 4\zeta\right). \tag{C3}$$

Needles ($\alpha \gg 1$). Series expansions for large α and small ζ yield

$$\nu_{0,\text{crit}}^{\text{HF}} \sim \frac{1}{8}\left(7 - \sqrt{29}\right) + \frac{551 + 91\sqrt{29}}{1392}\zeta \simeq 0.202 + 0.748\,\zeta. \tag{C4}$$